Noise Reduction in Magnetic Resonance Images using Wave Atom Shrinkage

J.Rajeesh   rajeesh_j@yahoo.co.in
Senior Lecturer/Department of ECE
Noorul Islam College of Engineering
Kumaracoil, 629180, India

R.S.Moni   moni2006_r_s@yahoo.co.in
Professor/Department of ECE
Noorul Islam University
Kumaracoil, 629180, India

S.Palanikumar   palanikumarcsc@yahoo.com
Assistant Professor/Department of IT
Noorul Islam University
Kumaracoil, 629180, India

T.Gopalakrishnan   gopalme@gmail.com
Lecturer/Department of ECE
Noorul Islam University
Kumaracoil, 629180, India

Abstract

De-noising is always a challenging problem in magnetic resonance imaging and important for clinical diagnosis and computerized analysis, such as tissue classification and segmentation. It is well known that the noise in magnetic resonance imaging has a Rician distribution. Unlike additive Gaussian noise, Rician noise is signal dependent, and separating signal from noise is a difficult task. An efficient method for enhancement of noisy magnetic resonance image using wave atom shrinkage is proposed. The reconstructed MRI data have high Signal to Noise Ratio (SNR) compared to the curvelet and wavelet domain de-noising approaches.

Keywords: De-noising, Gaussian noise, Magnetic Resonance Images, Rician noise, Wave Atom Shrinkage.

1. INTRODUCTION

De-noising of magnetic resonance (MR) images remains a critical issue, spurred partly by the necessity of trading-off resolution, SNR, and acquisition speed, which results in images that still demonstrate significant noise levels [1]–[7]. Sources of MR noise [8] include thermal noise (from the conductivity of the system's hardware), inductive losses (from the conductivity of the object being imaged), sample resolution, and field-of-view (among others). Understanding the spatial distribution of noise in an MR image is critical to any attempt to estimate the underpinning (true) signal. The investigation of how noise is distributed in MR images (along with techniques proposed to ameliorate the noise) has a long history. It was shown that pure noise in MR

magnitude images could be modeled as a Rayleigh distribution [1]. Afterwards, the Rician model [4] was proposed as a more general model of noise in MR images. Reducing noise has always been one of the standard problems of the image analysis. The success of many analysis techniques such as segmentation, classification depends mainly on the image being noiseless.

Magnetic Resonance Imaging (MRI) is a notable medical imaging technique that has proven to be particularly valuable for examination of the soft tissues in the body. MRI is an imaging technique that makes use of the phenomenon of nuclear spin resonance. Since the discovery of MRI, this technology has been used for many medical applications. Because of the resolution of MRI and the technology being essentially harmless it has emerged as the most accurate and desirable imaging technology [9]. MRI is primarily used to demonstrate pathological or other physiological alterations of living tissues and is a commonly used form of medical imaging. Despite significant improvements in recent years, magnetic resonance (MR) images often suffer from low SNR or Contrast-to-Noise Ratio (CNR), especially in cardiac and brain imaging. This is problematic for further tasks such as segmentation of important features, three-dimensional image reconstruction, and registration. Therefore, noise reduction techniques are of great interest in MR imaging as well as in other imaging modalities.

This paper presents a de-noising method in Magnetic Resonance Images using Wave Atom Shrinkage that leads to the improvement of SNR in low and high noise level images. The paper is organized with sections as follows. In section II, the work related to this paper is briefly explained, In section III, the theoretical concepts of wavelet transform, curvelet transform and wave atom transforms are described, in section IV, the application of wave atom transform, curvelet transform and wavelet transforms to MRI and observations are discussed. In section V, the paper is concluded by briefly explained the pros and corns of the proposed method.

2. RELATED WORKS

The image processing literature presents a number of de-noising methods based on Partial Differential Equations (PDEs) [10], including some of them concentrated on MR Images [11] – [14]. Even though these methods have the advantage of simplicity and removal of stair case effect that occurs with the TV-norm filter. Such methods, however, impose certain kinds of models on local image structure that are often too simple to capture the complexity of anatomical MR images. Further, these methods entail manual tuning of critical free parameters that control the conditions under which the models prefer one sort of structure to another. These factors have been an impediment to the widespread adoption of PDE-based techniques for processing MR images.

Another approach to image restoration is nonparametric statistical methods. For instance, in [15], [16] propose an unsupervised information-theoretic adaptive filter, namely UINTA, that relies on nonparametric MRF models derived from the corrupted images. UINTA restores images by generalizing the mean-shift procedure [17], [18] to incorporate neighborhood information. They show that entropy measures on first-order image statistics are ineffective for de-noising and, hence, advocate the use of higher-order/Markov statistics. UINTA, however, does not assume a specific noise model during restoration. In [19], [20] proposed a de-noising strategy along similar lines, namely NL-Means, but one relying on principles in nonparametric regression.

Recently, many of the popular de-noising algorithms suggested are based on wavelet thresholding [21]–[24]. These approaches attempt to separate significant features/signals from noise in the frequency domain and simultaneously preserve them while removing noise. If the wavelet transform is applied on MR magnitude data directly, both the wavelet and the scaling coefficients of a noisy MRI image become biased estimates of their noise-free counterparts. Therefore, it was suggested [22] that the application of the wavelet transform on squared MR magnitude image data (which is noncentral chi-square distributed) would result in the wavelet

coefficients no longer being biased estimates of their noise-free counterparts. Although the bias still remains in the scaling coefficients, it is not signal-dependent and can therefore be easily removed [22], [24]. The difficulty with wavelet or anisotropic diffusion algorithms is again the risk of over-smoothing fine details particularly in low SNR images [25].

From points discussed above, it is understood that all the algorithms have the drawback of over-smoothing fine details. In [26], stated that oscillatory functions or oriented textures have a significantly sparser expansion in wave atoms than in other fixed standard representations like Gabor filters, wavelets and curvelets. Due to the signal dependent mean of the Rician noise, one can overcome this problem by filtering the square of the noisy MR magnitude image in the transformed coefficients [22].

3. THEORY

3.1. Wavelet
Wavelet bases are bases of nested function spaces, which can be used to analyze signals at multiple scales. Wavelet coefficients carry both time and frequency information, as the basis functions varies in position and scale. The fast wavelet transform (FWT) efficiently converts a signal to its wavelet representation [27]. In a one-level FWT, a signal is split into an approximation part and a detail part. In a multilevel FWT, each subsequent is split into an approximation and detail. For 2-D images, each subsequent is split into an approximation and three detail channels as horizontally, vertically, and diagonally oriented details, respectively. The inverse FWT (IFWT) reconstructs each subsequent from approximation and detail channels. If the wavelet basis functions do not have compact support, the FWT is computed most efficiently in the frequency domain. This transform and its inverse are called the Fourier-wavelet decomposition (FWD) and Fourier-wavelet reconstruction (FWR), respectively.

Assume that the observed data

$$X(t) = S(t) + N(t) \tag{1}$$

contains the true signal $S(t)$ with additive noise $N(t)$ as functions in time t to be sampled. Let $W(.)$ and $W{-}1(.)$ denote the forward and inverse wavelet transform operators. Let $D(., \lambda)$ denote the de-noising operator with hard threshold λ. To wavelet shrinkage de-noise $X(t)$ in order to recover $\hat{S}(t)$ as an estimate of $S(t)$. Then the three steps

      1. Take the forward transform $Y = W(X)$ (2)

      2. Apply shrinkage $Z = D(., \lambda)$ (3)

      3. Take inverse transform $\hat{S} = W^{-1}(Z)$ (4)

summarize the procedure. For implementation MATLAB functions were used with db5 wavelet and the decomposition level depends upon the row size of the image (i.e. If the row size is N, then the decomposition level becomes $\log_2 N$).

3.2. Curvelet
The curvelet transform, like the wavelet transform, is a multiscale transform, with frame elements indexed by scale and location parameters. Unlike the wavelet transform, it has directional parameters, and the curvelet pyramid [28][29] contains elements with a very high degree of directional specificity. The elements obey a special scaling law, where the length of the support of a frame elements and the width of the support are linked by the relation width = length^2. Curvelets are interesting because they efficiently address very important problems where wavelets are far from ideal.

For example, Curvelets provide optimally sparse representations of objects, which display curve-punctuated smoothness except for discontinuity along a general curve with bounded curvature. Such representations are nearly as sparse as if the object were not singular and turn out to be far sparser than the wavelet decomposition of the object.

This phenomenon has immediate applications in approximation theory and in statistical estimation. In approximation theory, let f_m be the m-term curvelet approximation (corresponding to the m largest coefficients in the curvelet series) to an object $f(x_1, x_2) \in L^2(R^2)$. Then the enhanced sparsity says that if the object f is singular along a generic smooth C^2 curve but otherwise smooth, the approximation error obeys

$$\|f - f_m\|_{L^2}^2 \leq C.(\log m)^3 . m^{-2} \tag{5}$$

and is optimal in the sense that no other representation can yield a smaller asymptotic error with the same number of terms. The implication in statistics is that one can recover such objects from noisy data by simple curvelet shrinkage and obtain a MSE in order of magnitude better than what is achieved by more traditional methods. In fact, the recovery is asymptotically near optimal. The statistical optimality of the curvelet shrinkage extends to other situations involving indirect measurements as in a large class of ill-posed inverse problems [30]. For implementation software, we refer to the home page http://www.curvelet.org due to Demanet and Ying.

3.2. Waveatom
Demanet and Ying [31] introduced so-called wave atoms, that can be seen as a variant of 2-D wavelet packets and obey the parabolic scaling of curvelets wavelength= (diameter) [2]. Oscillatory functions or oriented textures (e.g., fingerprint, seismic profile, engineering surfaces) have a significantly sparser expansion in wave atoms than in other fixed standard representations like Gabor filters, wavelets, and curvelets.

Wave atoms have the ability to adapt to arbitrary local directions of a pattern, and to sparsely represent anisotropic patterns aligned with the axes. In comparison to curvelets, wave atoms not only capture the coherence of the pattern along the oscillations, but also the pattern across the oscillations.

In the following, we shortly summarize the wave atom transform as recently suggested in [31]. See also [32] for a very related approach.

Consider a 1-D family of wave packets $\psi_{m,n}^j(x)$, $j \geq 0, m \geq 0, n \in N$, centered in frequency around $\pm w_{j,m} = \pm \pi 2^j m$ with $c_1 2^j \leq m \leq c_2 2^j$ (where $c_1 < c_2$ are positive constants) and centered in space around $x_{j,n} = 2^{-j} n$. For that purpose, let g be a real valued C^∞ bumb function with compact support in $\left[-7\pi/6, 5\pi/6\right]$ such that for $|\omega| \leq \pi/3$

$$g\left(\frac{\pi}{2} - \omega\right)^2 + g\left(\frac{\pi}{2} + \omega\right) = 1 \tag{6}$$

$$g\left(-\frac{\pi}{2} - 2\omega\right)^2 = g\left(\frac{\pi}{2} + \omega\right) \tag{7}$$

Then the function $\hat{\psi}_m^0(\omega)$ is determined by the formula

$$e^{-\omega/2}\left[e^{i\alpha m} g\left(e_m\left(\omega - \pi\left(m + \frac{1}{2}\right)\right)\right) + e^{-i\alpha m} g\left(e_{m+1}\left(\omega + \pi\left(m + \frac{1}{2}\right)\right)\right)\right] \tag{8}$$

where $e_m = (-1)^m$ and $\alpha_m = (\pi/2)(m + (1/2))$. The properties of g have to ensure that

$$\sum_{m=0}^{\infty} \left|\hat{\psi}_m^0(\omega)\right|^2 = 1 \tag{9}$$

Then the translates $\left\{\psi_m^0(.-n)\right\}$ form an orthonormal basis of $L^2(R)$. Introducing the basis functions

$$\psi_{m,n}^j(x) = \psi_m^j(x - 2^{-j}n) = 2^{j/2}\psi_m^0(2^j x - n) \tag{10}$$

The transform $WA: L^2(R) \to l^2(Z)$ maps a function u onto a sequence of wave atom coefficients

$$c_{j,m,n} = \int_{-\infty}^{\infty} u(x)\psi_{m,n}^j(x)dx = \frac{1}{2\pi}\int_{-\infty}^{\infty} e^{-i2^{-j}n\omega} \overline{\psi_m^j(\omega)} \hat{u}(\omega)d\omega \tag{11}$$

In the 2-D case, Let $\mu = (j,m,n)$, where $m = (m_1, m_2)$ and $n = (n_1, n_2)$. We consider

$$\varphi_\mu^+(x_1, x_2) = \psi_{m_1,n_1}^j(x_1)\psi_{m_2,n_2}^j(x_2) \tag{12}$$

and the Hilbert transformed wavelet packets

$$\varphi_\mu^-(x_1, x_2) = \psi_{m_1,n_1}^j(x_1)\psi_{m_2,n_2}^j(x_2) \tag{13}$$

Where for decomposition

$\psi_{m,n}(\omega) = \psi_{m,n,+}^j(\omega) + i\psi_{m,n,-}^j(\omega)$ with $\psi_{m,n,-}^j(\omega) = \overline{\psi_{m,n,+}^j(\omega)}$ and the Hilbert transform is defined by

$$H\hat{\psi}_{m,n}^j(\omega) = -i\psi_{m,n,+}^j(\omega) + i\psi_{m,n,-}^j(\omega) \tag{14}$$

(Note that the above decomposition of $\hat{\psi}_{m,n}$ is possible since $\psi_{m,n}$ is real-valued). A recombination

$$\psi_\mu^{(1)} = \frac{\psi_\mu^+ + \psi_\mu^-}{2}, \psi_\mu^{(2)} = \frac{\psi_\mu^- + \psi_\mu^-}{2} \tag{15}$$

provides basis functions with two bumps in the frequency plane being symmetric with respect to the origin. Together, $\psi_\mu^{(1)}$ and $\psi_\mu^{(2)}$ form a wave atom frame, and the wave atom coefficients $C_u^{(1)}, C_u^{(2)}$ are the scalar products of u with $\psi_\mu^{(1)}$ and $\psi_\mu^{(2)}$.

In [31], a discretization of this transform is described for the 1-D case, as well as an extension to two dimensions. The algorithm is based on the fast Fourier transform and a wrapping trick. For implementation software, we refer to the homepage http://www.waveatom.org/software.html due to Demanet and Ying.

The wave atom shrinkage can be formulated as a hard threshold function given by

$$\theta_h(x) = \begin{cases} x - \dfrac{\sigma^2}{x}, & |x| \geq \sigma \\ 0, & |x| < \sigma \end{cases} \tag{16}$$

Where σ is the standard deviation, estimated by histogram based techniques.

4. EXPERIMENTS AND RESULTS

This section gives a detailed qualitative and quantitative analysis of the proposed MRI de-noising algorithm. It compares the performance of the proposed method with wavelet shrinkage and curvelet shrinkage. It is evaluated with simulated images and real images.

4.1. Simulated Images

To validate the proposed method with simulated images, images were down loaded from Brainweb[33]. Rician noise is generated by adding independent and identically distributed (i.i.d.) additive Gaussian noise with the noise free image and, subsequently, taking the magnitude of the resulting complex-valued image [34]. Noisy image with different values of standard deviation are applied on the proposed de-noising method and the Signal to Noise ratio (SNR) [34] is obtained by

$$SNR = 10\log_{10}(\text{var}(x)/\text{var}(\hat{x} - x)) \qquad (17)$$

where x is noise free simulated image and $\hat{x}$ is noisy image or de-noised image.

The shrinkage is obtained by

$$X_\sigma u = T^{-1}\theta T(u) \qquad (18)$$

where T denotes the transform and T^{-1} denotes the inverse transform, θ is taken as a threshold function defined by a fixed threshold $\sigma > 0$.

Analysis is made with four conditions vide i) fixed high SNR for various threshold ii) fixed low SNR for various threshold iii) fixed low threshold for various SNR and iv) fixed high threshold for various SNR

i) The chosen SNR is 19.0505 dB and the threshold is varied from 0.03 to 0.3. The observations are given in Fig 1. It shows the wave atom shrinkage gives higher SNR on all threshold values compared to wavelet shrinkage and curvelet shrinkage. The performances of the models are given in Fig 2 for the threshold 0.06.

ii) The chosen SNR is 9.21 dB and the threshold is varied from 0.03 to 0.3. The observations are given in Fig 3. It shows the wave atom shrinkage gives higher SNR on all threshold values compared to wavelet shrinkage and curvelet shrinkage except for the threshold 0.03,0.06 and 0.3, where the curvelet shrinkage perform well. The performances of the models are given in Fig 4. for the threshold 0.24.

iii) Here the threshold is fixed at 0.06 and SNR is varied from 9.37 dB to 19.12 dB. It shows the proposed method increases the SNR to the maximum of 16.6% compared to wavelet by 14.6% and curvelet by 8%. The analysis is presented in Fig 5.

iv) Here the threshold is fixed at 0.24 and SNR is varied from 9.26 dB to 18.87 dB. It shows the proposed method increases the SNR to the maximum of 57% compared to wavelet by 52% and curvelet by 52%. The analysis is presented in Fig 6.

It is observed that the performance of all filters depends on the proper selection of threshold value and the SNR of the noisy image. Also, the performance of the proposed method is better with the maximum increase of 57% SNR compared to the methods given in [35] like anisotropic diffusion by 34% and UINTA by 18.1% increase of SNR.
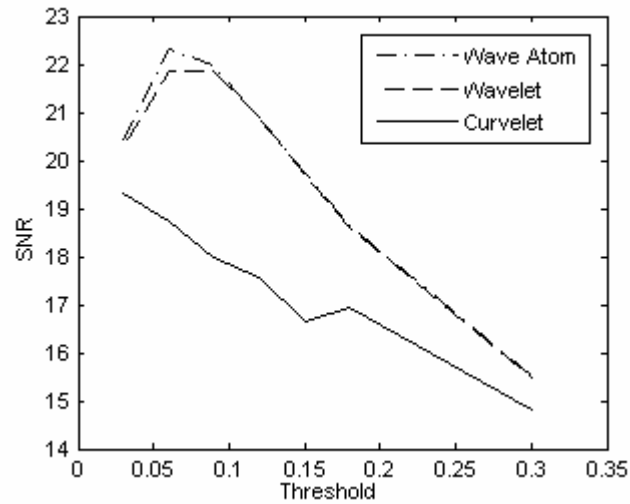
FIGURE 1: De-noised image SNR for high SNR noisy image.

(a) SNR=19.00dB

(b) SNR=22.21dB

(c) SNR=21.83dB

(d) SNR=19.23dB
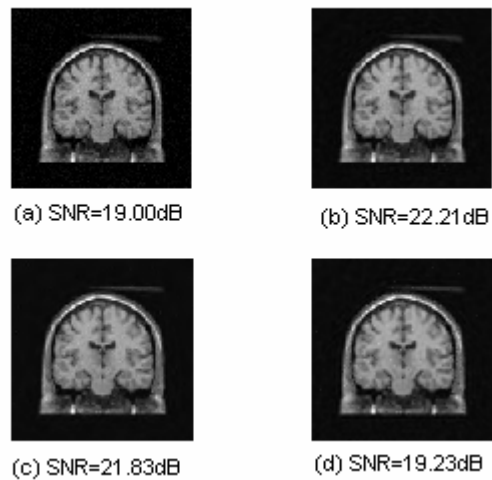
FIGURE 2: High SNR images (a) Noisy image (b) De-noised using Wave Atom (c) De-noised using Wavelet (d) Den-noised using Curvelet.
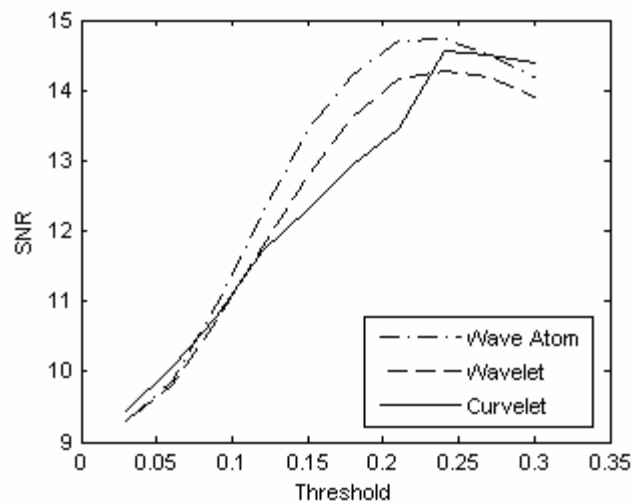
FIGURE 3: De-noised image SNR for low SNR noisy image.

(a) SNR=9.20dB   (b) SNR=14.78dB

(c) SNR=14.38dB   (d) SNR=14.2dB
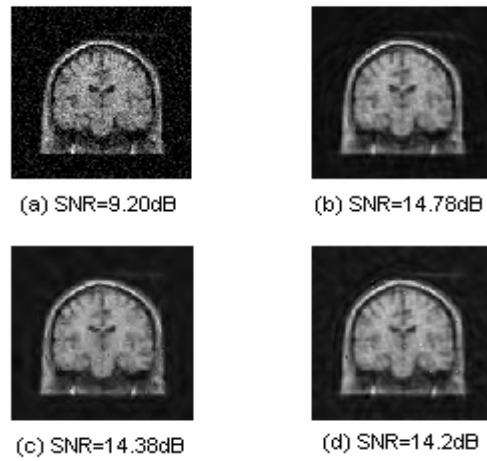
FIGURE 4: Low SNR images (a) Noisy image (b) De-noised using Wave Atom (c) De-noised using Wavelet (d) Den-noised using Curvelet.
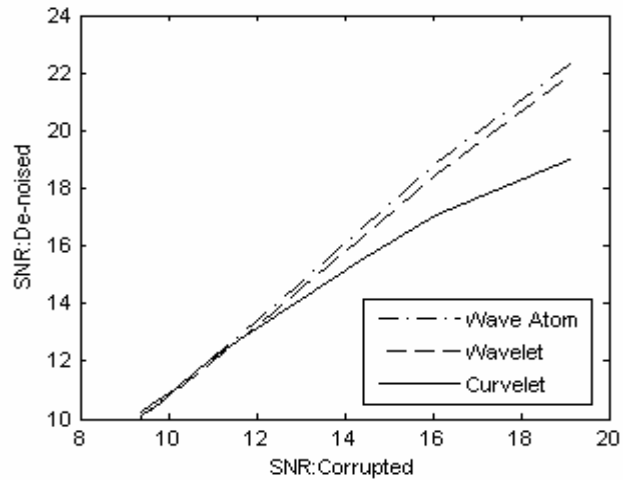
FIGURE 5: Performance between noisy and de-noised images with the threshold of 0.06.
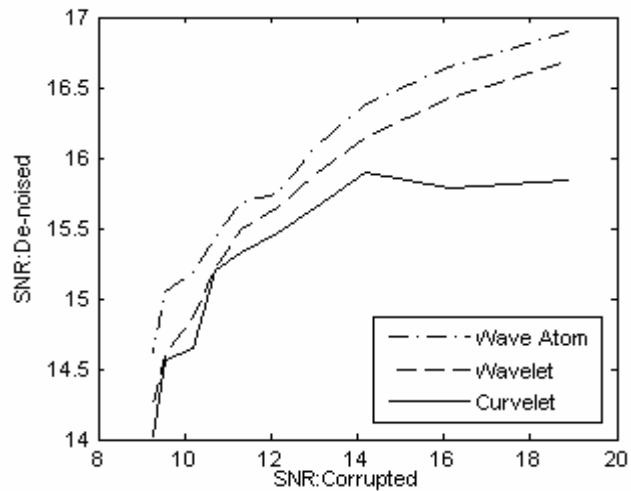
FIGURE 6: Performance between noisy and de-noised images with the threshold of 0.24

4.2. Real Images

Fig. 7 show the performance of the proposed method and the wavelet and curvelet shrinkage on corrupted MR images of adult human brains taken from Sree Chitra Tirunal Institute of Medical Sciences, Thiruvananthapuram, where the MRI scans were acquired on a 1.5T Vision System (Siemens, Erlangen, Germany). T1-weighted magnetization prepared rapid gradient echo (MP-RAGE) with the following specifications: FOV = 224, matrix = 256 x 256, resolution = 1 x 1 x 1.25 mm^3, TR = 9.7 ms, TE = 4ms, flip angle = 10, TI = 20 ms, TD = 200ms. The voxel size of the image is 0.781x0.781x2mm^3. The proposed method is able to recover the image features to a significant extent, qualitatively, despite a significant level of intensity inhomogeneity apparent in some images. The medical doctors validated the images.
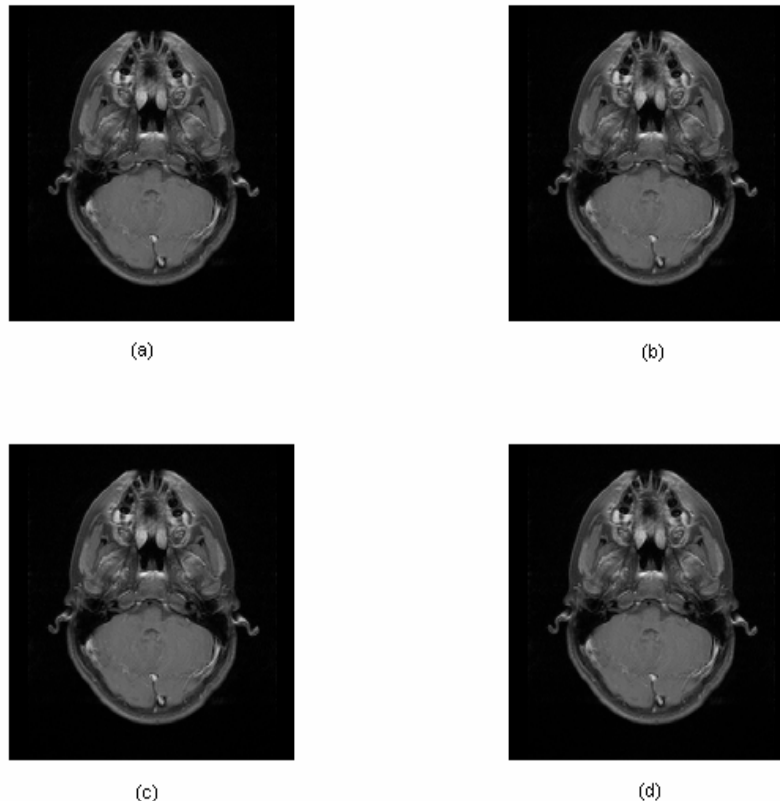
FIGURE 7: Real (a) Noisy image (b) De-noised using Wave Atom (c) De-noised using Wavelet (d) Den-noised using Curvelet

5. CONCLUSION

A novel scheme is proposed for the de-noising of Magnetic Resonance Images using wave atom shrinkage. It is proved that the proposed approach achieves a better SNR compared to wavelet and curvelet shrinkages. The edge preserving property is clearly an advantage of the proposed method. Further, including a large dataset of real-time normal and pathological MR images will emphasize the efficiency of proposed method. The next work is to analyze the performance of the proposed method on other modalities of MRI such as T2 and PD.

6. REFERENCES

1. W. A. Edelstein, P. A. Bottomley, and L. M. Pfeifer.A signal-to-noise calibration procedure for nmr imaging systems. Med. Phys 1984;11:2:180–185.

2. E. R. McVeigh, R. M. Henkelman, and M. J. Bronskill. Noise and filtration in magnetic resonance imaging. Med. Phys 1985;12:5:586–591.

3. R. M. Henkelman. Measurement of signal intensities in the presence of noise in mr images. Med. Phys 1985;12:2:232–233.

4. M. A. Bernstein, D. M. Thomasson, and W. H. Perman. Improved detectability in low signal-to-noise ratio magnetic resonance images by means of phase-corrected real construction. Med. Phys 1989;16:5:813–817.

5. M. L. Wood, M. J. Bronskill, R. V. Mulkern, and G. E. Santyr. Physical MR desktop data. Magn Reson Imaging 1994;3:19–24.

6. H. Gudbjartsson and S. Patz. The Rician distribution of noisy MRI data. Magn Reson Med 1995;34:6:910–914.

7. A. Macovski. Noise in MRI. Magn Reson Med 1996;36:3:494–497.

8. W. A. Edelstein, G. H. Glover, C. J. Hardy, and R. W. Redington. The intrinsic SNR in NMR imaging. Magn Reson Med 1986;3:4:604–618.

9. G.A. Wright. Magnetic Resonance Imaging. IEEE Signal Processing Magazine 1997;1:56-66.

10. X. Tai, K. Lie, T. Chan, and S. Osher, Eds. Image Processing based on Partial Differential Equations 2005; New York: Springer.

11. G. Gerig, O. Kubler, R. Kikinis, and F. A. Jolesz. Nonlinear anisotropic filtering of MRI data. IEEE Trans Med Imag 1992;11:2:221–232.

12. M. Lysaker, A. Lundervold, and X. Tai. Noise removal using fourth-order partial differential equation with applications to medical magnetic resonance images in space and time. IEEE Trans Image Process 2003;12:12:1579–1590.

13. A. Fan, W. Wells, J. Fisher, M. Çetin, S. Haker, R. Mulkern, C. Tempany, and A.Willsky. A unified variational approach to denoising and bias correction in MR. Inf Proc Med Imag 2003;148–159.

14 S. Basu, P. T. Fletcher, and R. T. Whitaker. Rician noise removal in diffusion tensor MRI. Med Imag Comput Comput Assist Intervention 2006;117–125.

15. S. P. Awate and R. T. Whitaker. Higher-order image statistics for unsupervised, information-theoretic, adaptive, image filtering. Proc IEEE Int Conf. Comput Vision Pattern Recognition 2005;2:44–51.

16 S. P. Awate and R. T. Whitaker. Unsupervised, information-theoretic, adaptive image filtering for image restoration. IEEE Trans Pattern Anal Mach Intell 2006;28:3:364–376.

17. K. Fukunaga and L. Hostetler. The estimation of the gradient of a density function, with applications in pattern recognition. IEEE Trans Inf Theory 1975;21:1:32–40.

18. D. Comaniciu and P. Meer. Mean shift: A robust approach toward feature space analysis. IEEE Trans Pattern Anal Mach Intell 2002;24:5:603–619.

19. A. Buades, B. Coll, and J. M. Morel. A non-local algorithm for image denoising. IEEE Int Conf Comp Vis Pattern Recog 2005;2:60–65.

20. A. Buades, B. Coll, and J. M. Morel. A review of image denoising algorithms, with a new one. Multiscale Modeling Simulation 2005;4:2:490–530.

21. J. B. Weaver, Y. Xu, D. M. Healy Jr., and L. D. Cromwell. Filtering noise from images with wavelet transforms. Magn Reson Med 1991;21:2:288–295.

22. R. D. Nowak. Wavelet-based Rician noise removal for magnetic resonance imaging. IEEE Trans Image Process 1999;8:10:1408–1419.

23. A. M. Wink and J. B. T. M. Roerdink. Denoising functional MR images: A comparison of wavelet denoising and Gaussian smoothing. IEEE Trans Image Process 2004;23:3:374–387.

24. A. Pizurica, A. M. Wink, E. Vansteenkiste, W. Philips, and J. B. T. M. Roerdink. A review of wavelet denoising in MRI and ultrasound brain imaging. Current Med Imag Rev 2006;2:2:247–260.

25. D. Tisdall and M. S. Atkins. MRI denoising via phase error estimation. Proc SPIE Med Imag 2005;646–654.

26. Gerlind Plonka and Jianwei Ma. Nonlinear Regularised Reaction-Diffusion Filter for Denoising of Images with Textures. IEEE Trans. Image Processing 2008;17:8:1283–1294.

27. S. G. Mallat. A theory for multiresolution signal decomposition: The wavelet representation. IEEE Trans Pattern Anal Machine Intell 1989;l:11:674–693.

28. E. J. Candès and D. L. Donoho. Curvelets. [Online] Available: http://www-stat.stanford.edu/~donoho/Reports/1999/Curvelets.pdf.
29. M. N. Do and M. Vetterli. Framing pyramids. IEEE Trans Signal Proc 2003;2329–2342.

30. E. J. Candes and D. L. Donoho. Recovering edges in ill-posed inverse problems: Optimality of Curvelet frames. Ann. Statist. 30 (2002); 784 –842.
31. L. Demanet and L. Ying. Wave atoms and sparsity of oscillatory patterns. Appl Comput Harmon Anal 2007;23:3:368–387.

32. G. Cottet and L. Germain. Image processing through reaction combined with nonlinear diffusion. Math Comput 1993;61:659–673.

33. [Online]. Available: http://www.bic.mni.mcgill.ca/brainweb/
34. A. Pizurica, W. Philips, I. Lemahieu, and M. Acheroy. A versatile wavelet domain noise filtration technique for medical imaging. IEEE Trans Med Imag 2003;22:3:323–331.
35. Suyash P. Awate and Ross T. Whitaker. Feature-Preserving MRI Denoising: A Nonparametric Empirical Bayes Approach. IEEE Trans Med Imag 2007;26:9:1242–1255.